Hindawi
Journal of Nanomaterials
Volume 2020, Article ID 7826231, 9 pages
https://doi.org/10.1155/2020/7826231

Research Article

Chemosensing Test Paper Based on Aggregated Nanoparticles of a Barbituric Acid Derivative

Jinzhen Xu,[1] Hanjun Zhang,[1] Zhen Xu,[1] Furong Tao,[1] Yuezhi Cui,[1] and William W. Yu[2]

[1]*School of Chemical and Pharmaceutical Engineering, Qilu University of Technology (Shandong Academy of Sciences), Jinan 250353, China*
[2]*Louisiana State University, Shreveport, Louisiana 71115, USA*

Correspondence should be addressed to Yuezhi Cui; yuezhicui@163.com and William W. Yu; wyu6000@gmail.com

Received 1 May 2020; Revised 25 June 2020; Accepted 10 July 2020; Published 1 August 2020

Guest Editor: Xiao Jin

The development of sensitive, cheap, and portable methods for detecting nitroaromatics explosives has a profound significance and value for public health and environmental protection. For this purpose, a new D-π-A barbituric acid derivative CB-CYH with aggregation-induced emission (AIE) behavior was synthesized, which can interact with picric acid through photoinduced electron transfer (PET). Scanning electron microscopy (SEM) and dynamic light scattering (DLS) indicate that the enhanced emission of the compounds is related to the formation of nano-aggregates. It is well known that an important source of mechanochromic fluorescence (MCF) characteristic materials is the compound with AIE characteristics. The chemosensing test paper prepared by aggregated nanoparticles based on AIE properties is often subjected to external friction or squeeze during transportation or storage, resulting in changes of their optical properties, and destruction of test paper followed. Therefore, the development of compounds with AIE properties and stable optical properties in the presence of external stimuli is particularly important for chemosensing test paper. Molecular dynamics simulation (MDS) shows that the presence of hydrophobic cycloalkyl group in CB-CYH, which caused the molecules to be closely interspersed with each other; hence, it is difficult to change the microstructure and stacking mode of molecules by external stimulation simultaneously; the optical properties are not changed by external stimuli. Therefore, the test paper based on the AIE effect of CB-CYH was developed as chemosensing test paper for the detection of nitroaromatics.

1. Introduction

The problem of human health is threatened by explosive residues from terrorist bombings, and military exercises are becoming more and more serious. The nitroaromatics are commonly used as explosive materials, and the methods of detection of nitroaromatic explosives are various [1], such as metal detectors [2], thermal neutron analysis [3], electrochemical assays [4], Raman spectroscopy [5], gas chromatography [6], X-ray imaging [7], and mass spectrometry [8]. However, the disadvantages are obvious, such as time-consuming, or expensive, or complicated processing. So many researchers turn their attention to photoluminescence (PL) sensor [9–12], which is a low-cost with high-sensitivity, easy-to-operate, and a new type of very promising method. The PL sensor is usually based on a photoinduced electron transfer (PET) mechanism that is from an electron-rich group of the sensor to an electron-deficient nitroaromatic. However, the practical application of traditional PL sensor is hindered by the phenomenon of aggregation quenching (ACQ) [13].

Since Tang's group [14–16] discovered compounds with aggregate-induced emission (AIE) feature, more and more people have paid attention to this; these compounds can not only be widely used in luminescent polymers, explosive detection [17, 18], mechanochromic fluorescence [19], optoelectronic materials, biosensors, and gels but also successfully solve the ACQ problem [20–28]. Compounds with AIE properties are nonluminous when dissolved in a good solvent but are completely opposite in the aggregated state. The reason for strong emission in the aggregate state is that the formation of aggregated nanoparticles restricted intramolecular

rotation (RIR), the nonradiative channels are blocked and radiation paths are opened [29]. PL sensors based on AIE have successfully solved the problems of traditional sensors with ACQ properties.

Chemosensing test papers are widely used due to their portability, low price, and easy storage [30–32]. It is well known that an important source of mechanochromic fluorescence (MCF) characteristic materials is the compounds with AIE characteristics. Chemosensing test paper based on AIE properties is often subjected to external friction or squeeze during transportation or storage, resulting in changes in their optical properties. Fortunately, a new D-π-A barbituric acid derivative CB-CYH with aggregation-induced emission (AIE) behavior was synthesized, of which the optical properties are not changed by external stimuli. Hence, the chemosensing test paper was prepared by aggregated nanoparticles of CB-CYH, which was developed for the detection of nitroaromatics.

2. Experimental Section

2.1. Materials. 1,3-Dicyclohexylurea, dimethylformamide, malonyl chloride, and 9-phenyl-9H-carbazole (A.R., 99%) were purchased from Jiu ding Chemical, and which without further purification. DMF is usually dried sequentially by molecular sieves (4 Å), CaH_2 and sodium sand successively, and distilled prior to use.

2.2. Characterizations. UV-vis spectra were registered by UV-2500 spectrometer. Emission spectra were recorded on an F-4600 fluorescence spectrophotometer. ^{1}H NMR (400 MHz) spectra were recorded on AVANCE II 400 spectrometer. FT-IR spectra were measured by a Nicolet 380 spectrometer using the KBr pellet method.

2.3. Computation. The optimizations and electronic structure calculation for the CB-CYH were done at B3LYP/def2-SVP level with Gaussian09 software. Solvation effects were incorporated by molecular dynamics simulations (MDS) [33] solvation models with water as solvent. The dispersion correction was conducted by Grimme's D3 version with BJ damping function [34].

Eight optimized molecules of CB-CYH were randomly dissolved in 400 water molecules, respectively, to form initial systems with the same cubic simulation lattice ($x = 28.89$ Å, $y = 28.89$ Å, and $z = 28.89$ Å). Subsequently, all-atomic molecular dynamics simulations (MDS) were performed for the system in BIOVIA Materials Studio 2019 Forcite packages. The simple point charge (SPC) model [35, 36], which can accurately describe the water solution environment [37], is adopted for all water molecules.

The MD simulation of all systems can be performed after charges and potentials are assigned to each atom. The long-range electrostatic interactions have been accounted for using the Ewald method. The total energy is written as a combination of valence terms including diagonal and off-diagonal cross-coupling terms and nonbond interaction terms, which include the Coulombic and Lennard-Jones functions for electrostatic and van der Waals interactions,

$$E = E_{\text{bonds}} + E_{\text{angles}} + E_{\text{dihedrals}} + E_{\text{cross}} + E_{\text{VDW}} + E_{\text{elec}}, \quad (1)$$

where E_{VDW} and E_{elec} are given by the Eq. (2):

$$E_{\text{non-bond}} = E_{\text{VDW}} + E_{\text{elec}} = \sum \varepsilon_{ij} \left[2\left(\frac{\sigma_{ij}}{r_{ij}}\right)^9 - 3\left(\frac{\sigma_{ij}}{r_{ij}}\right)^6 \right] + \sum \frac{q_i q_j}{r_{ij}}. \quad (2)$$

The MDS was performed using the COMPASS force field [38, 39], which is a force field for atomistic simulation of common organic molecules based on the state-of-the-art ab initio and empirical parametrization techniques. The simulations were equilibrated at constant temperature (298.15 K) and volume (NPT) for 30 ns.

2.4. Synthesis of Compounds. The synthetic routes of CB-CYH which include are illustrated in Scheme 1. In addition to this, the synthesis step of 1,3-dicyclohexylbarbituric acid (1) and 9-phenyl carbazole-3-carbaldehyde (2) can be found from Ref. [40, 41], respectively.

2.4.1. Synthesis of CB-CYH. A mixture of 2 (3 mmol) and 1 (3 mmol) in (10 ml) EtOH was refluxed for 4 hr. After filtration, the filtrate was concentrated under reduced pressure and purified by column chromatography (ethyl acetate : petroleum ether = 2 : 1). Production: 90%. ^{1}H NMR (400 MHz, Chloroform-*d*) δ 8.35 (s, 1H), 8.14 (d, $J = 8.8$ Hz, 2H), 7.36 (t, $J = 7.8$ Hz, 4H), 7.21 (d, $J = 7.6$ Hz, 6H), 6.95 (d, $J = 8.7$ Hz, 2H), 4.74 (dd, $J = 14.0$, 10.5 Hz, 2H), 2.37 (q, $J = 12.5$ Hz, 4.H), 1.84 (s, 3H), 1.67 (s, 4H), 1.42-1.33 (m, 4H), 1.31-1.22 (m, 3H) (Figure S1) FT-IR (KBr): 1669 cm^{-1} (C=O) (Figure S2). HRMS (ESI) *m/z*: $[M + H]^+$ calcd for $C_{35}H_{35}N_3O_3$, 545.38328; found, 545.27512 (Figure S3). ^{13}C NMR (126 MHz, Chloroform-*d*) δ 163.54, 161.57, 156.45, 1482.84, 145.37, 138.22, 129.60, 128.72, 127.25, 126.59, 115.47, 55.15, 29.39, 25.67, 25.12 (Figure S4).

3. Results and Discussion

3.1. Optical Properties. The absorption and emission spectra for CB-CYH are presented in Figure 1(a). The maximum absorption wavelength of CB-CYH was at 421 nm, which can be attributed to the intramolecular charge transfer (ICT) [42] from the carbazole group to the barbituric acid group, which can also be confirmed by density functional theory (DFT) calculations (Figure 1(b)). It should note that the absorption peak at 230-350 nm belongs to the π-π * electron transition of the corresponding benzene ring unit. In dilute THF solution, CB-CYH showed dim emission with emission wavelengths at 517 nm.

The AIE property of CB-CYH was studied in THF/H_2O system. As shown in Figure 2(a), the emission intensity of CB-CYH increased by 4.4 folds with f_w increased from 0% to 80%, because of the formation of nano-aggregates; however, as the f_w increases further, the emission intensity decreases, which is due to the the low solubility of CB-CYH

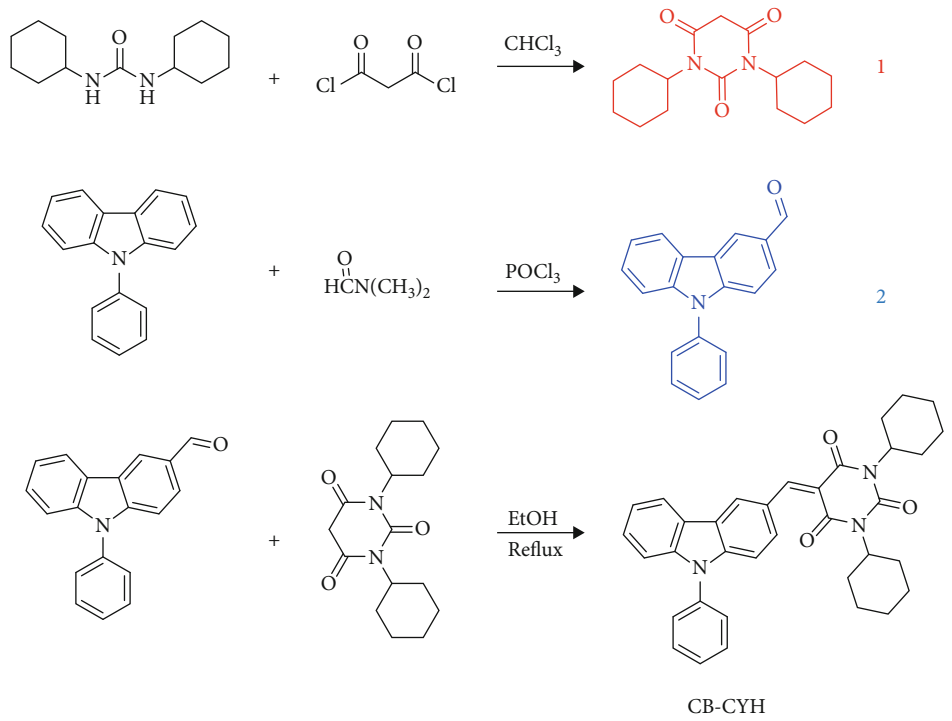

Scheme 1: Synthetic routes to CB-CYH.

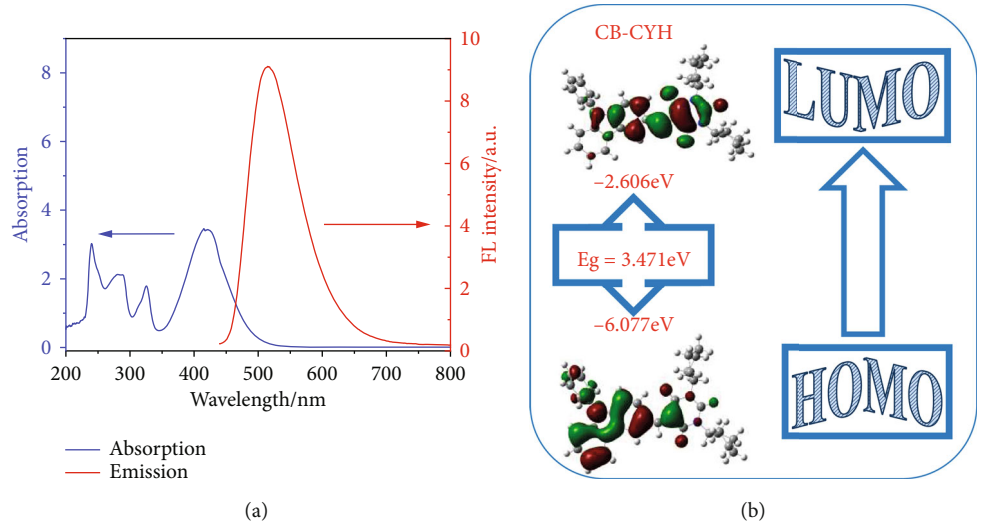

(a) (b)

Figure 1: (a) UV-visible absorption spectrum and emission spectrum of CB-CYH in pure THF (10^{-4} M). (b) Electron density distributions of LUMO and HOMO molecular orbitals of CB-CYH calculated by the B3LYP/6-31Gd program. (HOMO: the highest occupied molecular orbital energy; LUMO: the lowest unoccupied molecular orbital energy).

at high water content, resulting in rapid precipitation of the compounds, the total number of emission molecules decreases in the solution, and fluorescence reduction follows [43]. Fluorescent photograph of CB-CYH in THF/H_2O mixtures with different f_w, irradiated by 365 nm wavelength also demonstrate that CB-CYH is AIE active compound.

The fluorescence quantum yields of pure solution and aggregate state are determined relative to coumarin 307 in ethanol solution as a quantum yield standard (ΦF (fluorescence quantum yield) = 56%). The coumarin 307 is selected as a standard to study the ΦF due to its maximum absorption and emission wavelength (395 nm and 500 nm, respectively), which are close to the synthesized AIE compounds in this work; the fluorescence quantum yields of compound in the pure solution and aggregate state are 1.8% and 7.4%, respectively.

Scanning electron microscopy (SEM) and dynamic light scattering (DLS) were used to detect the morphology and size of nano-aggregates in f_w = 80% (Figure 3) which show the presence of spherical and blocky aggregates. As shown in

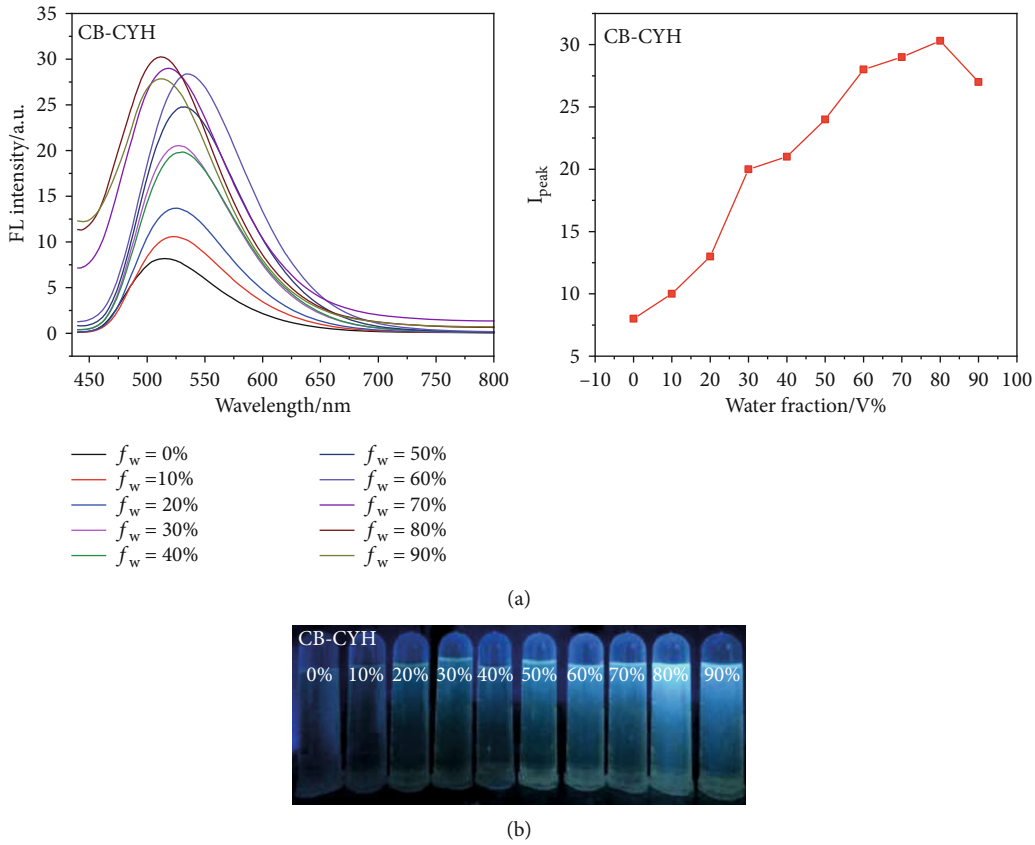

Figure 2: (a) Fluorescence spectrum of CB-CYH in THF/H_2O mixtures with different f_w. (b) Fluorescent photograph of CB-CYH in THF/H_2O mixtures with different f_w, irradiated by 365 nm wavelength.

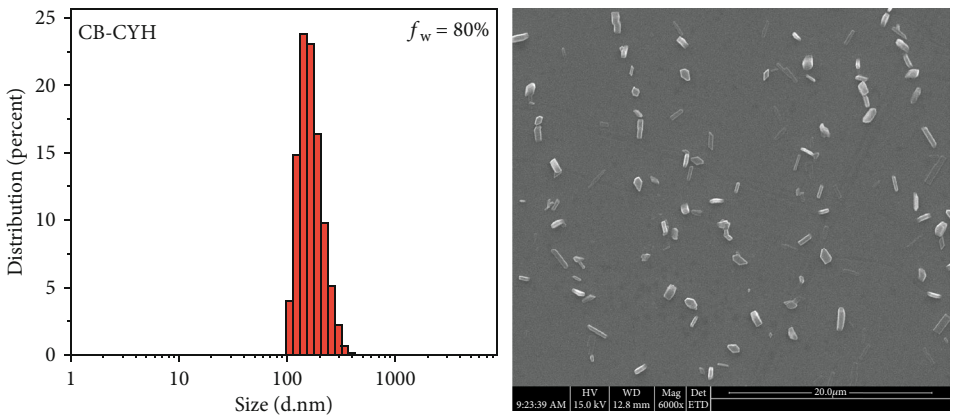

Figure 3: SEM images and particle size distribution histograms of CB-CYH in a THF/H_2O mixture (f_w = 80%) (solution concentration: 10^{-4} M).

Figure 3, the solution was uniformly stable at a water content of 80%, and the average diameters (d) of the CB-CYH aggregates was 180 nm, respectively. These data indicate that the enhanced emission of the compound is related to the formation of nano-aggregates.

As shown in Figure S5, The fluorescence intensity of CB-CYH (f_w = 80%) did not change within 30 minutes. These results mean that CB-CYH (f_w = 80%) has excellent photostability. In addition, the average diameter (d) of CB-CYH aggregate has basically no change within half an hour (Figure S6).

It is well known that an important source of mechanochromic fluorescence (MCF) property materials are compounds with AIE properties. However, it can be seen from Figure 4(a) that there is almost no change in color and fluorescence after grinding of CB-CYH; simultaneously,

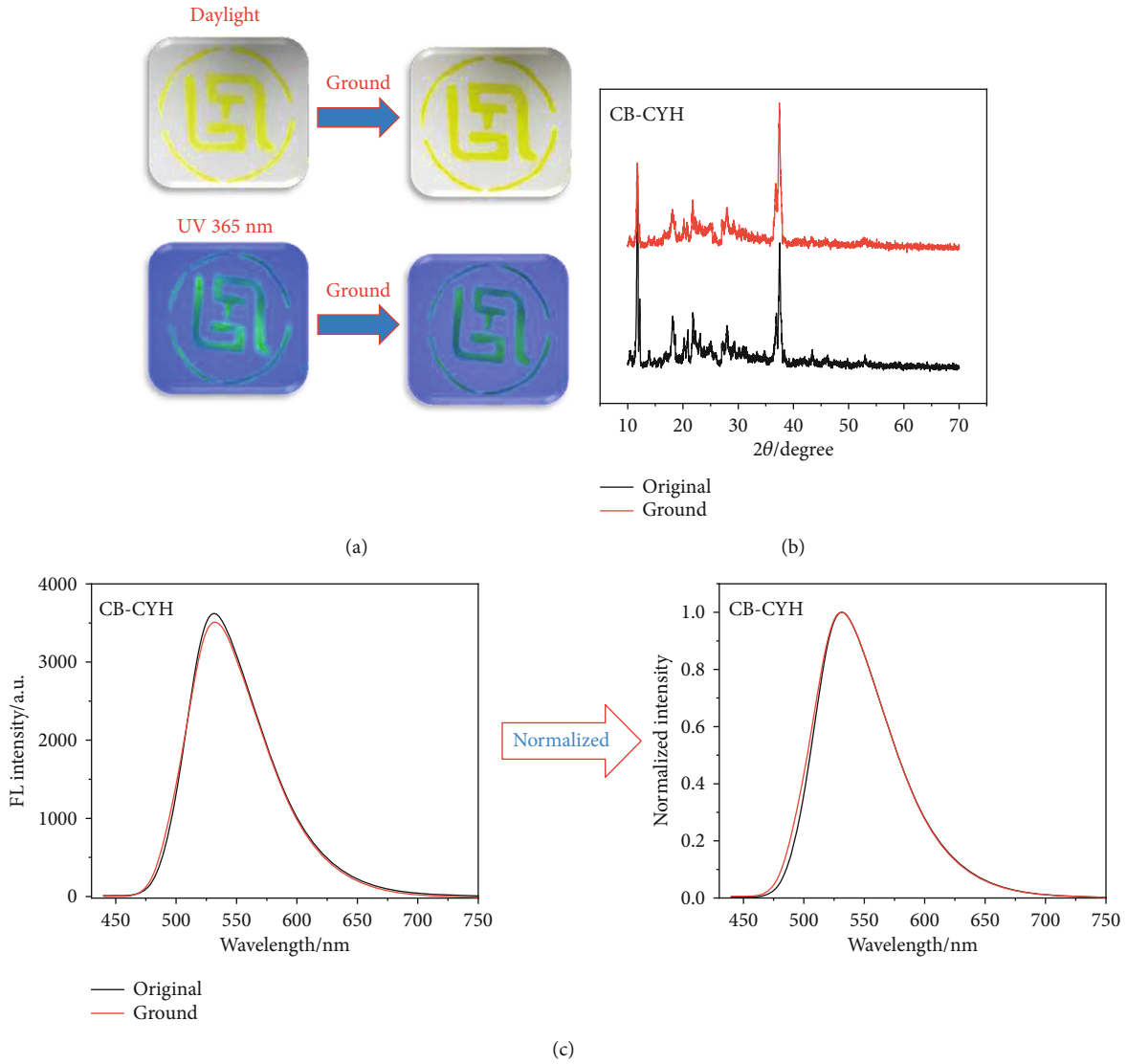

FIGURE 4: (a) Photographs of colour and fluorescence of CB-CYH in original and ground under daylight and UV 365 nm. (b) XRD patterns of CB-CYH in original and ground. (c) Left: fluorescence spectrum of CB-CYH of solid powder in original and ground. Right: normalized fluorescence spectrum of CB-CYH of solid powder in original and ground.

the XRD diffraction peak of CB-CYH almost unchanged (Figure 4(b)). It can also be seen from Figure 4(c) that the emission spectrum of CB-CYH has almost no change before and after grinding, regardless of the emission wavelength or intensity. The structure of the CB-CYH showed strong distortion, but not MCF property, which inspired our intense curiosity.

3.2. Molecular Dynamics Simulations (MDS). The behavior of CB-CYH in the aggregated state was studied by MDS. As shown in Figure 5(a), all the molecules of the formed nanoaggregates together under high water content, and at the same time, the structure of CB-CYH shows a strong deformation. Among them, the electron repulsion and strong intermolecular interactions between aryl rings in carbazoles lead to extremely curved configurations (Figure 5(b)), and from the distribution of dihedral angles between several moieties, the main dihedral angles of angle-1, angle-2, and angle-3 are 50°, 155°, and 155°, respectively. Meanwhile, the cyclohexane on the N atom of the barbiturate acid exhibits extremely distorted chair conformation, which further increases the degree of distortion of the molecule CB-CYH (Figure 5(c)). These data indicate that the molecule takes 3D conformation, which makes it easy to pack closely in the crystalline state. As shown in Figure 4(d), because of hydrophobic interactions, the substituents cyclohexane in CB-CYH tend to aggregate together. Hydrophobic interactions pull all molecules together and spread each other, which formed aggregated nanoparticles to lock the molecules. This also proves why CB-CYH does not have MCF property.

3.3. Chemosensing Test Paper. The chemosensing test paper was prepared by soaking Whatman filter paper in CB-CYH ($f_w = 80\%$) (10^{-4} M) solution (aggregated nanoparticles) and then dried it in the air stream. Picric acid (PA) was selected as representative of nitroaromatic explosives. First,

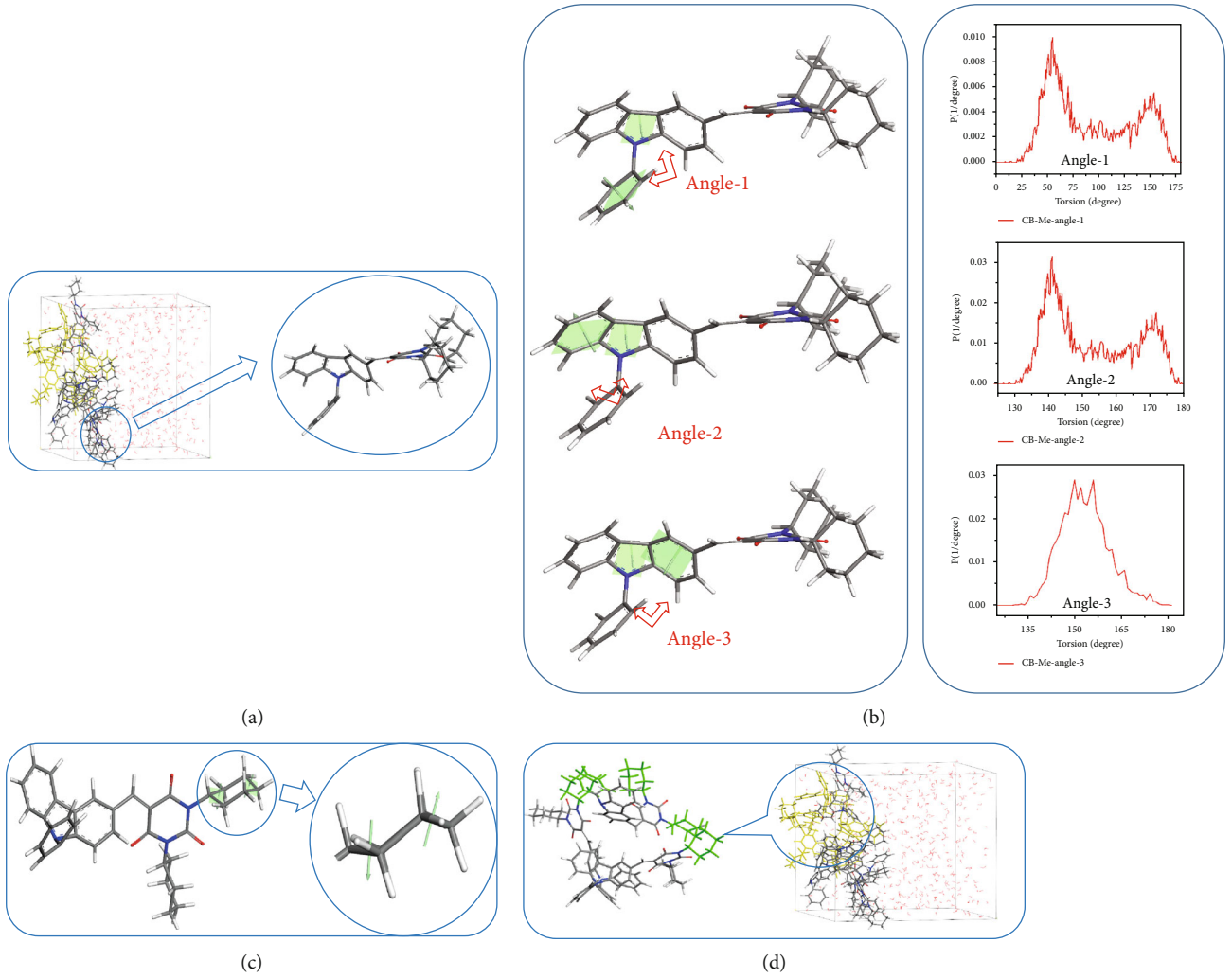

Figure 5: (a) The molecule conformation and aggregation structure of CB-CYH by MDS. (b) Dihedral angle of the substituted carbazole in CB-CYH. (c) Configurations of substituted cyclohexane on the N atom of barbituric acid in CB-CYH. (d) Hydrophobic force of cyclohexane in CB-CYH.

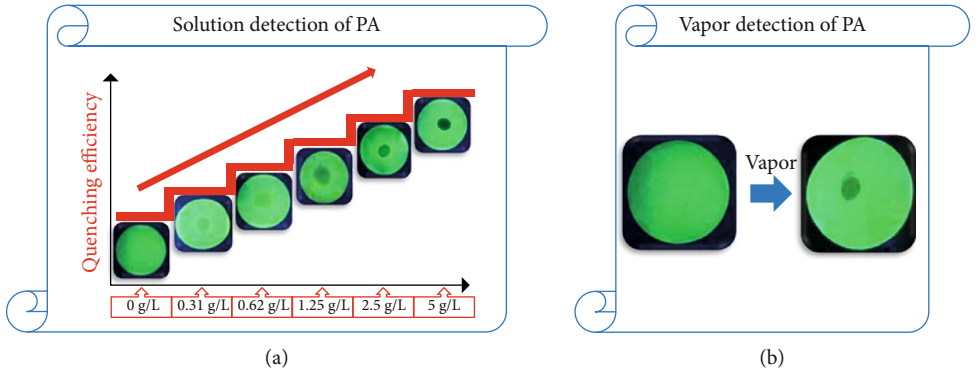

Figure 6: Paper test. (a) Solution mode detection of PA. (b) Gas phase mode detection of PA.

the PA test was performed at solution state. As shown in Figure 6(a), the test paper emits bright blue-green fluorescence without adding PA solution, when adding 0.31 g/L PA solution, the test paper shows a slight quenching. It is found that the quenching efficiency increases with the increase of PA concentration, when the concentration reaches to 5 g/L, the area of adding PA solution is completely quenched. Next, perform a steam mode test. Place the chemical sensing test paper in a cylindrical glass container filled with solid PA (0.2 g) maintained at a constant temperature

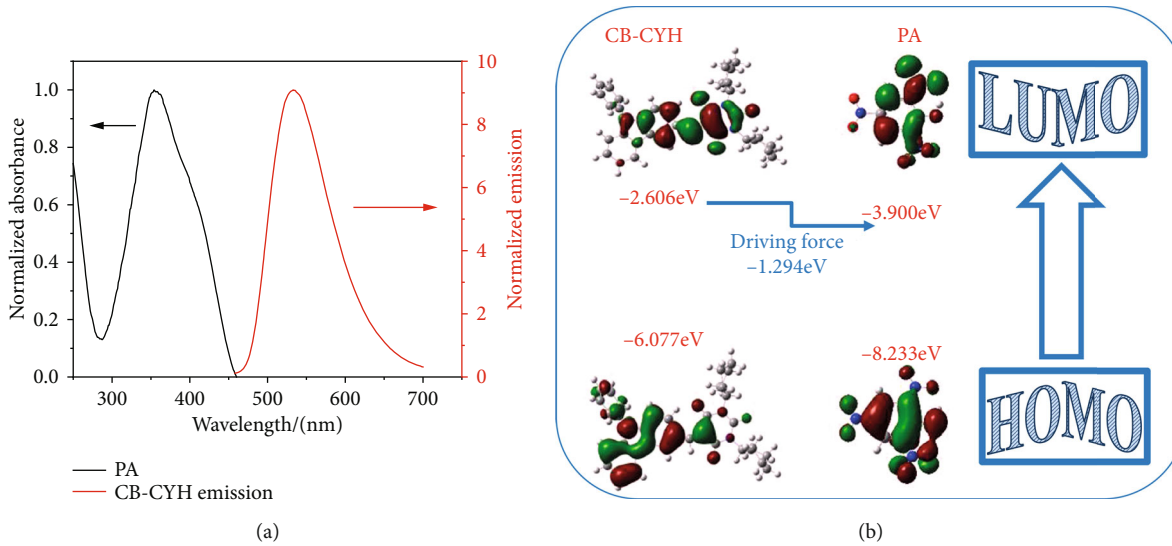

Figure 7: (a) Absorption spectrum of PA and emission spectrum of CB-CYH. (b) Energy levels, energy gaps, and electron cloud distributions of the HOMO and LUMO of PA and CB-CYH calculated by the B3LYP/6-325 31G (d) program.

of 45°C for 5 minutes (under standard atmospheric pressure). The circular area of the test paper was exposed to PA vapor. It can be seen from Figure 6(b) that the fluorescence of the test paper is significantly quenched in the area exposed to the PA vapor. These results showed that CB-CYH-based chemosensing test paper can detect picric acid.

3.3.1. Sensing Mechanism. As shown in Figure 7, the absorption spectrum of PA and emission spectrum of CB-CYH were tested, which to explore the quenching mechanism. It noticed from Figure 7(a) that the absorption spectrum of PA and the emission spectrum of CB-CYH hardly overlap, and the results showed that the quenching mechanism of CB-CYH was photoinduced electron transfer (PET) [44–46].

In explosives containing nitro groups, which has a strong electron-withdrawing ability, resulting in that is extremely deficient in electrons. However, the fluorescent compound as the electron-donor is rich in electrons, and it is easy to interact with the electron-deficient substance by charge transfer interaction and bind under the condition of light irradiation. In the process of the photoinduced electron transfer (PET) mechanism, the fluorescent material provides electrons to the ground state of the electron-deficient nitroaromatic explosive, and part of it will return to the ground state in the form of a complex, thus losing fluorescence. Some electrons will return to the electron donor and still emit fluorescence. The driving force for the PET mechanism is the difference between the LUMO energy levels between the donor and acceptor, namely, the size of the energy gap difference.

As shown in Figure 7(b), the energy levels and electron cloud distributions of the HOMO and LUMO of TNT and CB-CYH were calculated by the B3LYP/6-325 31G (d) program. When the excited CB-CYH is exposed to TNT, the excited electrons are transferred from the LUMO of CB-CYH to the LUMO of PA. The main driving force of PET is the difference between the LUMO value of CB-CYH and PA, which is -1.924 eV.

4. Conclusions

In summary, the chemosensing test paper was prepared by aggregated nanoparticles of CB-CYH, which was developed for the detection of nitroaromatics. MDS showed that CB-CYH with a strong twist structure cannot cause changes in fluorescence, color, and emission wavelength by external stimuli due to the close interpenetration between molecules. Hence, the chemosensing test paper will not be damaged by squeeze and friction during transportation and storage.

Data Availability

The data used to support the findings of this study are available from the corresponding author upon request.

Conflicts of Interest

The authors declare that they have no conflicts of interest.

Acknowledgments

This work was financially supported by the Natural Science Foundation of Shandong Province (ZR2018MB025), a Project of Shandong Province Higher Educational Science and Technology Program (NO. J18KZ004), and the Funds for Research Leader in Jinan (2018GXRC028).

Supplementary Materials

In the supplementary materials mainly included with 1H NMR, 13C NMR, FT-IR, and mass spectra of CB-CYH, light stability of CB-CYH nano-aggregates, and particle size distribution of CB-CYH in a THF/H2O mixture (fw = 80%). Figure S1. 1H NMR of CB-CYH in Chloroform-d. Figure S2. FT-IR spectra of CB-CYH. Figure S3. HRMS spectra of CB-CYH. Figure S4. 13C NMR of CB-CYH in Chloroform-d. Figure S5. CB-CYH light stability in nano-aggregates state.

Figure S6. Particle size distribution histograms of CB-CYH in a THF/H2O mixture (fw = 80%) was left at room temperature for half an hour (solution concentration: 10-4 M). *(Supplementary Materials)*

References

[1] H. Zhou, M. H. Chua, B. Z. Tang, and J. Xu, "Aggregation-induced emission (AIE)-active polymers for explosive detection," *Polymer Chemistry*, vol. 10, no. 28, pp. 3822–3840, 2019.

[2] J. M. Sylvia, J. A. Janni, J. D. Klein, and K. M. Spencer, "Surface-enhanced Raman detection of 2, 4-dinitrotoluene impurity vapor as a marker to locate landmines," *Analytical chemistry*, vol. 72, no. 23, pp. 5834–5840, 2000.

[3] W. Dong, S. Xue, P. Lu et al., "Functionality of peripheral side chain for enhanced performance of conjugated polymer-F8BT as an example," *Journal of Polymer Science Part A: Polymer Chemistry*, vol. 49, no. 21, pp. 4549–4555, 2011.

[4] H. Ma, L. Yao, P. Li, O. Ablikim, Y. Cheng, and M. Zhang, "Highly sensitive and selective fluorometric/electrochemical dual-channel sensors for TNT and DNT explosives," *Chemistry-A European Journal*, vol. 20, no. 37, pp. 11655–11658, 2014.

[5] G. A. Eiceman and J. A. Stone, "Ion Mobility Spectrometers in National defence," *Analytical Chemistry*, vol. 76, no. 21, pp. 390A–397A, 2004.

[6] K. Håkansson, V. Ramal, A. Coorey Roman, L. Zubarev Victor, and T. P. Håkansson, "Low-mass ions observed in plasma desorption mass spectrometry of high explosives," *Journal of mass spectrometry*, vol. 35, no. 3, pp. 337–346, 2000.

[7] S. F. Hallowell, "Screening people for illicit substances: a survey of current portal technology," *Talanta*, vol. 54, no. 3, pp. 447–458, 2001.

[8] J. C. Mathurin, T. Faye, A. Brunot, J. C. Tabet, G. Wells, and C. Fuché, "High-pressure ion source combined with an in-axis ion trap mass spectrometer. 1. Instrumentation and applications," *Analytical chemistry*, vol. 72, no. 20, pp. 5055–5062, 2000.

[9] N. Venkatramaiah, S. Kumar, and S. Patil, "Fluoranthene based fluorescent chemosensors for detection of explosive nitroaromatics," *Chemical Communications*, vol. 48, no. 41, pp. 5007–5009, 2012.

[10] N. Venkatramaiah, S. Kumar, and S. Patil, "Femtogram detection of explosive nitroaromatics: fluoranthene-based fluorescent chemosensors," *Chemistry-A European Journal*, vol. 18, no. 46, pp. 14745–14751, 2012.

[11] H. Nie, Y. Lv, L. Yao et al., "Fluorescence detection of trace TNT by novel cross-linking electropolymerized films both in vapor and aqueous medium," *Journal of Hazardous Materials*, vol. 264, pp. 474–480, 2014.

[12] K. R. Ghosh, S. K. Saha, and Z. Y. Wang, "Ultra-sensitive detection of explosives in solution and film as well as the development of thicker film effectiveness by tetraphenylethene moiety in AIE active fluorescent conjugated polymer," *Polymer Chemistry*, vol. 5, no. 19, pp. 5638–5643, 2014.

[13] B. Chen, Y. Jiang, B. He et al., "Synthesis, structure, photoluminescence, and electroluminescence of siloles that contain planar fluorescent chromophores," *Chemistry - An Asian Journal*, vol. 9, no. 10, pp. 2937–2945, 2014.

[14] M. H. Chua, H. Zhou, T. T. Lin, J. Wu, and J. W. Xu, "Aggregation-induced emission active 3, 6-bis (1, 2, 2-triphenylvinyl) carbazole and bis (4-(1, 2, 2-triphenylvinyl) phenyl) amine-based poly (acrylates) for explosive detection," *Journal of Polymer Science Part A: Polymer Chemistry*, vol. 55, no. 4, pp. 672–681, 2017.

[15] H. Zhou, X. Wang, T. T. Lin, J. Song, B. Z. Tang, and J. Xu, "Poly (triphenyl ethene) and poly (tetraphenyl ethene): synthesis, aggregation-induced emission property and application as paper sensors for effective nitro-compounds detection," *Polymer Chemistry*, vol. 7, no. 41, pp. 6309–6317, 2016.

[16] H. Zhou, Q. Ye, W. T. Neo et al., "Electrospun aggregation-induced emission active POSS-based porous copolymer films for detection of explosives," *Chemical Communications*, vol. 50, no. 89, pp. 13785–13788, 2014.

[17] K. Li, R. H. Yu, C. M. Shi, F. R. Tao, T. D. Li, and Y. Z. Cui, "Electrospun nanofibrous membrane based on AIE-active compound for detecting picric acid in aqueous solution," *Sensors and Actuators B: Chemical*, vol. 262, pp. 637–645, 2018.

[18] D. Ding, K. Li, B. Liu, and B. Z. Tang, "Bioprobes based on AIE fluorogens," *Accounts of Chemical Research*, vol. 46, no. 11, pp. 2441–2453, 2013.

[19] Z. Zhao, B. He, and B. Z. Tang, "ChemInform Abstract: Aggregation-Induced Emission of Siloles," *Cheminform*, vol. 46, no. 45, pp. 5347–5365, 2015.

[20] H. Zhou, J. Li, M. H. Chua, H. Yan, B. Z. Tang, and J. Xu, "Poly (acrylate) with a tetraphenylethene pendant with aggregation-induced emission (AIE) characteristics: highly stable AIE-active polymer nanoparticles for effective detection of nitro compounds," *Polymer Chemistry*, vol. 5, no. 19, pp. 5628–5637, 2014.

[21] W. Z. Yuan, Z.-Q. Yu, Y. Tang et al., "High solid-state efficiency fluorescent main chain liquid crystalline polytriazoles with aggregation-induced emission characteristics," *Macromolecules*, vol. 44, no. 24, pp. 9618–9628, 2011.

[22] H.-J. Zhang, Y. Tian, F.-r. Tao et al., "Detection of nitroaromatics based on aggregation induced emission of barbituric acid derivatives," *Spectrochimica Acta Part A: Molecular and Biomolecular Spectroscopy*, vol. 222, pp. 117168–117168, 2019.

[23] H. Zhang, Y. Cui, F. Tao, D. Zhang, Z. Xu, and L. Guo, "Multi-purpose barbituric acid derivatives with aggregation induced emission," *Spectrochimica Acta Part A: Molecular and Biomolecular Spectroscopy*, vol. 223, pp. 1386–1425, 2019.

[24] R. Yoshii, K. Suenaga, K. Tanaka, and Y. Chujo, "Mechanofluorochromic materials based on aggregation-induced emission-active boron ketoiminates: regulation of the direction of the emission color changes," *Chemistry-A European Journal*, vol. 21, no. 19, pp. 7231–7237, 2015.

[25] J. Wang, J. Mei, R. Hu, J. Z. Sun, A. Qin, and B. Z. Tang, "Click synthesis, aggregation-induced emission, E/Z isomerization, self-organization, and multiple chromisms of pure stereoisomers of a tetraphenylethene-cored luminogen," *Journal of the American Chemical Society*, vol. 134, no. 24, pp. 9956–9966, 2012.

[26] X. Gu, G. Zhang, Z. Wang, W. Liu, L. Xiao, and D. Zhang, "A new fluorometric turn-on assay for alkaline phosphatase and inhibitor screening based on aggregation and deaggregation

of tetraphenylethylene molecules," *Analyst*, vol. 138, no. 8, pp. 2427–2431, 2013.

[27] P. Xue, B. Yao, J. Sun, Z. Zhang, and R. Lu, "Emission enhancement of a coplanar π-conjugated gelator without any auxiliary substituents," *Chemical Communications*, vol. 50, no. 71, pp. 10284–10286, 2014.

[28] Z. Zhu, J. Qian, X. Zhao et al., "Stable and size-tunable aggregation-induced emission nanoparticles encapsulated with nanographene oxide and applications in three-photon fluorescence bioimaging," *ACS Nano*, vol. 10, no. 1, pp. 588–597, 2015.

[29] D. Li, Y. Zhang, Z. Fan, J. Chen, and J. Yu, "Coupling of chromophores with exactly opposite luminescence behaviours in mesostructured organosilicas for high-efficiency multicolour emission," *Chemical Science*, vol. 6, no. 11, pp. 6097–6101, 2015.

[30] S. Li, Y. Shang, E. Zhao et al., "Color-tunable and highly solid emissive AIE molecules: synthesis, photophysics, data storage and biological application," *Journal of Materials Chemistry C*, vol. 3, no. 14, pp. 3445–3451, 2015.

[31] M. Wang, X. Liu, H. Lu, H. Wang, and Z. Qin, "Highly selective and reversible chemosensor for $Pd2^{+}$ detected by fluorescence, colorimetry, and test paper," *ACS Applied Materials & Interfaces*, vol. 7, no. 2, pp. 1284–1289, 2015.

[32] X. Yong, M. Su, W. Wang, Y. Yan, J. Qu, and R. Liu, "A naked-eye chemosensor for fluoride ions: a selective easy-to-prepare test paper," *Organic & Biomolecular Chemistry*, vol. 11, no. 14, pp. 2254–2257, 2013.

[33] A. V. Marenich, C. J. Cramer, and D. G. Truhlar, "Universal solvation model based on solute electron density and on a continuum model of the solvent defined by the bulk dielectric constant and atomic surface tensions," *The Journal of Physical Chemistry B*, vol. 113, no. 18, pp. 6378–6396, 2009.

[34] S. Grimme, S. Ehrlich, and L. Goerigk, "Effect of the damping function in dispersion corrected density functional theory," *Journal of Computational Chemistry*, vol. 32, no. 7, pp. 1456–1465, 2011.

[35] H. J. C. Berendsen, J. P. M. Postma, W. F. Van Gunsteren et al., *Intermolecular Forces*, B. Pullman, Ed., Reidel, Dordrecht, 1981.

[36] H. J. C. Berendsen, J. R. Grigera, and T. P. Straatsma, "The missing term in effective pair potentials," *Journal of Physical Chemistry*, vol. 91, no. 24, pp. 6269–6271, 1987.

[37] M. J. Wiedemair and T. S. Hofer, "Towards a dissociative SPC-like water model–probing the impact of intramolecular Coulombic contributions," *Physical Chemistry Chemical Physics*, vol. 19, no. 47, pp. 31910–31920, 2017.

[38] H. Sun, P. Ren, and J. R. Fried, "The COMPASS force field: parameterization and validation for phosphazenes," *Computational and Theoretical Polymer Science*, vol. 8, no. 1-2, pp. 229–246, 1998.

[39] H. Sun, "COMPASS: an ab initio force-field optimized for condensed-phase applications overview with details on alkane and benzene compounds," *The Journal of Physical Chemistry B*, vol. 102, no. 38, pp. 7338–7364, 1998.

[40] A. G. O'Brien, E. M. Ricci, and M. Journet, "Dehydration of an Insoluble Urea Byproduct Enables the Condensation of DCC and Malonic Acid in Flow," *Organic Process Research & Development*, vol. 22, no. 3, pp. 399–402, 2018.

[41] S. Xue, W. Liu, X. Qiu, Y. Gao, and W. Yang, "Remarkable isomeric effects on optical and optoelectronic properties of N-phenylcarbazole-capped 9, 10-divinylanthracenes," *The Journal of Physical Chemistry C*, vol. 118, no. 32, pp. 18668–18675, 2014.

[42] K. Li, Y. Zhang, B. Qiao et al., "Facile fabrication of AIE/AIEE-active fluorescent nanoparticles based on barbituric for cell imaging applications," *RSC Advances*, vol. 7, no. 48, pp. 30229–30241, 2017.

[43] K. Li, X. Su, Y. Wang et al., "D-π-A type barbituric derivatives: aggregation induced emission, mechanofluorochromic and solvatochromic properties," *Journal of Luminescence*, vol. 203, pp. 50–58, 2018.

[44] M. Natali, S. Campagna, and F. Scandola, "Photoinduced electron transfer across molecular bridges: electron-and hole-transfer superexchange pathways," *Chemical Society Reviews*, vol. 43, no. 12, pp. 4005–4018, 2014.

[45] M. Kaur, S. K. Mehta, and S. K. Kansal, "A fluorescent probe based on nitrogen doped graphene quantum dots for turn off sensing of explosive and detrimental water pollutant, TNP in aqueous medium," *Spectrochim Acta A Mol Biomol Spectrosc*, vol. 180, pp. 37–43, 2017.

[46] L. Yuan, W. Lin, K. Zheng, and S. Zhu, "FRET-based small-molecule fluorescent probes: rational design and bioimaging applications," *Accounts of Chemical Research*, vol. 46, no. 7, pp. 1462–1473, 2013.